


ORIGINAL ARTICLE

Open Access



Hierarchical CNNPID Based Active Steering Control Method for Intelligent Vehicle Facing Emergency Lane-Changing

Wensa Wang¹, Jun Liang^{1*} , Chaofeng Pan¹ and Long Chen¹

Abstract

To resolve the response delay and overshoot problems of intelligent vehicles facing emergency lane-changing due to proportional-integral-differential (PID) parameter variation, an active steering control method based on Convolutional Neural Network and PID (CNNPID) algorithm is constructed. First, a steering control model based on normal distribution probability function, steady constant radius steering, and instantaneous lane-change-based active for straight and curved roads is established. Second, based on the active steering control model, a three-dimensional constraint-based fifth-order polynomial equation lane-change path is designed to address the stability problem with supersaturation and sideslip due to emergency lane changing. In addition, a hierarchical CNNPID Controller is constructed which includes two layers to avoid collisions facing emergency lane changing, namely, the lane change path tracking PID control layer and the CNN control performance optimization layer. The scaled conjugate gradient backpropagation-based forward propagation control law is designed to optimize the PID control performance based on input parameters, and the elastic backpropagation-based module is adopted for weight correction. Finally, comparison studies and simulation/real vehicle test results are presented to demonstrate the effectiveness, significance, and advantages of the proposed controller.

Keywords Intelligent vehicle, Rear-end collision avoidance, Steering control, Dynamics model, Neural Network, PID control

1 Introduction

Given architectural changes in the automotive industry and the incorporation of multi-sensor electronics, a vehicle is no longer an isolated individual and is instead an intelligent terminal that can be interconnected with the outside world. In contrast to traditional vehicles, intelligent vehicles integrate various sensors (such as radar and cameras), controllers, actuators, and other components to achieve efficient perception of human-vehicle-road information and good control of the vehicle during

driving [1]. However, intelligent vehicle traffic accidents occur frequently, thereby raising serious questions regarding the safety of intelligent vehicles [2–4]. Statistics indicate that more than 80% of rear-end accidents are caused by drivers [5], and untimely and insensitive steering during emergencies is the main cause of accidents [6, 7]. In China's complicated road environment, especially in high-velocity driving scenarios, it is not possible for risk avoidance to be achieved in the rear-end collision transient state, which increases the probability of major accidents such as serial collisions [8].

Current research mainly focuses on intelligent vehicle rear-end early warnings [9], steering control [10, 11], emergency braking control [12–15], and trajectory tracking control [16–18]. Tawari et al. examined the accurate identification and evaluation technology of rear-end

*Correspondence:

Jun Liang
liangjun@ujs.edu.cn

¹ Automotive Engineering Research Institute, Jiangsu University, Zhenjiang 212013, China

risk and collision warning strategies, which is well verified in practical applications [9]. However, research on further treatment measures after a rear-end warning is not clear. Therefore, an active steering method based on model predictive control [10] is proposed although the calculation velocity is slow and the dynamic performance of the system is unsatisfactory. Hence, research proposed using the predictive value of the lateral force of the tire as a parameter for active steering control [11]. Many advanced control methods [19–23], such as sliding mode variable structure control and optimal control, are applied in research on emergency braking and steering control [24–26]. However, there is a paucity of research on intelligent vehicle active steering control in rear-end transients.

Given this assumption, vehicle cornering velocity, tire cornering angle, yaw rate, and other parameters are derived [27]. In a simulation experiment [28], the proposed sliding mode control method adequately controls the vehicle in the drift state. This is insufficient to intelligently control the movement of the uniform drift and track the time-varying curvature path. Therefore, the selection of prediction models is also a critical issue to consider in trajectory tracking control [29–33]. A trajectory tracking controller based on a 2-DOF driving model and a 14-DOF dynamics model is designed to prove that the complex dynamics model is not always an optimal choice [34–36]. In contrast, it is important to reasonably simplify the model and select constraints that satisfy the driving conditions. The control stability analysis of a constant acceleration yaw dynamics model is completed under a fixed curvature although the time-varying acceleration model and time-varying curvature trajectory are not considered [37–39]. An energy-shaping control method that analyzes the stability of the trajectory tracking control using a combination of roll and slip constraints during steering [40] is developed. The above study indicated that the dynamic model is reasonably simplified at the expense of a certain control accuracy to ensure real-time control in the process of risk avoidance.

During emergency steering, mechanisms including slow system response, steering angle overshoot, and concussion are important [23–25]. In a traditional proportional-integral-differential (PID) controller, it is necessary to adjust PID control parameters at a certain velocity when used for rear-end collision avoidance control. Hence, the PID parameters must be dynamically adjusted in response to velocity. Otherwise, it is subject to decreases in the control performance, increases in the overshoot, and oscillation, which significantly affect driving safety [41, 42].

To solve this challenging problem, a hierarchical Convolutional Neural Network and PID (CNNPID)

controller is constructed which comprises two layers, namely a lane-change path-tracking PID control layer, and a CNN control performance optimization layer. The error between the setting points of the lateral motion can be eliminated in the lane-change path-tracking PID control layer to accurately track the lane-changing path. In the CNN control performance optimization layer, the scaled conjugate gradient backpropagation-based forward propagation control law is designed to optimize the PID control performance based on parameter variation, and elastic backpropagation is adopted for weight correction.

The study has three main implications: First, a normal distribution probability function, steady constant radius steering, and instantaneous lane-change-based active steering control model for straight and curved roads are established. Second, based on the active steering control model, a three-dimensional constraint-based fifth-order polynomial equation lane-change path is designed such that the stability problem with supersaturation and sideslip due to emergency lane changing is successfully addressed. In addition, a Hierarchical CNNPID Controller for intelligent vehicles to avoid collisions facing emergency lane changing is constructed, and it comprises two layers: the lane change path tracking PID control layer and the CNN control performance optimization layer. The scaled conjugate gradient backpropagation-based forward propagation control law is designed to optimize the PID control performance according to the input parameters, and elastic backpropagation is adopted for weight correction.

The rest of this paper is organized as follows: The system model is presented in Section 2. Accordingly, a Three-Dimension Constraint-based fifth-order polynomial equation lane-change path is designed in Section 3. Furthermore, a Hierarchical CNNPID Controller is proposed in Section 4. Simulation examples are provided and discussed in Section 5. Finally, the conclusions are presented in Section 6.

2 System Model

2.1 Kinematic Model for Intelligent Vehicle

A vehicle kinematic model [12] is crucial to establish an active steering control model. To balance the complexity of the model and computational load, a four-DOF vehicle model is constructed, and the steering system is simplified as a linear relationship between the steering wheel and the front wheel angle. Figure 1 shows a schematic of the four-DOF vehicle model. To improve the effectiveness of the model, the following assumptions are included.

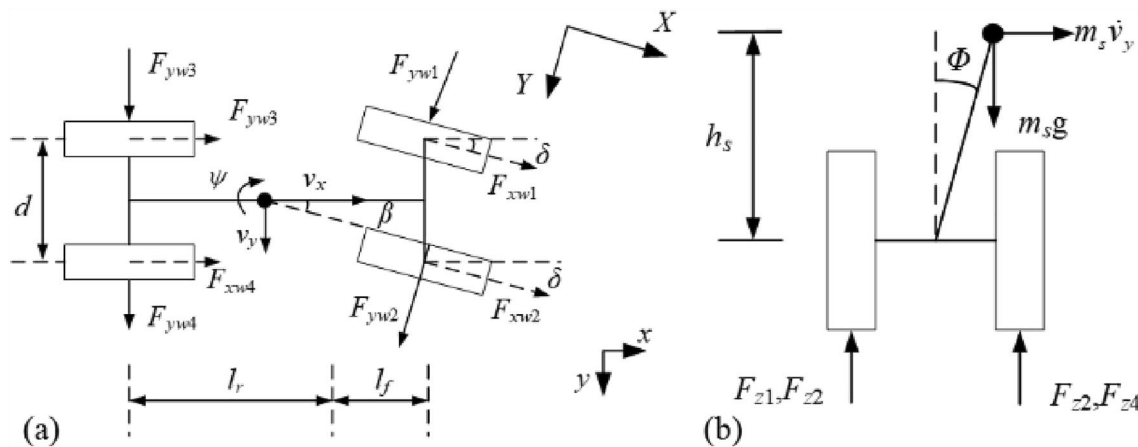


Figure 1 Schematic diagram of the four-DOFs vehicle: (a) Top view of the vehicle model, (b) Front view of the vehicle model

- 1) To ignore the vertical movement of the intelligent vehicle when driving on a flat road.
- 2) To ignore vehicle load transfer.
- 3) To ignore lateral and longitudinal aerodynamics.

The model has four degrees of freedom for chassis velocity: longitudinal velocity, lateral velocity, roll angular velocity, and yaw rate. The equations of motion for the system are expressed as follows:

$$\begin{cases} \sum F_{xi} = m_s(\dot{v}_x - v_y\dot{\psi}), \\ \sum F_{yi} = m_t(\dot{v}_y - v_x\dot{\psi}), \\ \sum M_{zi} = I_Z\ddot{\psi}, \end{cases} \quad (1)$$

$$\begin{cases} \sum F_{xi} = (F_{xw1} + F_{xw2}) \cos \delta - (F_{yw1} + F_{yw2}) \sin \delta + F_{xw3} + F_{xw4}, \\ \sum F_{yi} = (F_{xw1} + F_{xw2}) \sin \delta + (F_{yw1} + F_{yw2}) \cos \delta + F_{yw3} + F_{yw4}, \\ \sum M_{zi} = l_f [(F_{xw1} + F_{xw2}) \sin \delta + (F_{yw1} + F_{yw2}) \cos \delta] - l_f (F_{xw3} + F_{xw4}) \phi + \frac{d}{2} (F_{yw1} - F_{yw2}) \sin \delta - \frac{d}{2} (F_{xw1} - F_{xw2}) \cos \delta + \frac{d}{2} (F_{yw3} - F_{yw4}), \end{cases} \quad (2)$$

where M_{Zi} denotes moment on the z-axis; m_s and m_t denote the total sprung masses of the vehicle; v_x and v_y denote longitudinal and lateral velocities of the vehicle, respectively; I_Z denotes yaw moment; δ denotes the steering angle; F_{xwi} and F_{ywi} denote longitudinal and lateral forces.

Based on the kinematic model, an active steering control model is constructed to avoid rear-end collisions.

2.2 Active Steering Control Model to Avoid Collision Facing Emergency Lane-Changing

To address emergency lane-changing scenarios of vehicles on straight and curved roads, an active steering collision avoidance control model is constructed based on a normal distribution function, steady constant radius steering, and instantaneous lane change on straight and curved roads.

In Figure 2, the emergency lane-change behavior on curved roads consists of the following four stages: constant-radius steering, sinusoidal steering (turning left/right), sinusoidal steering (turning right/left), and constant-radius steering. When a vehicle is driving on a straight road, the lane-change behavior consists of only two sinusoidal steering stages. Therefore, lane-change

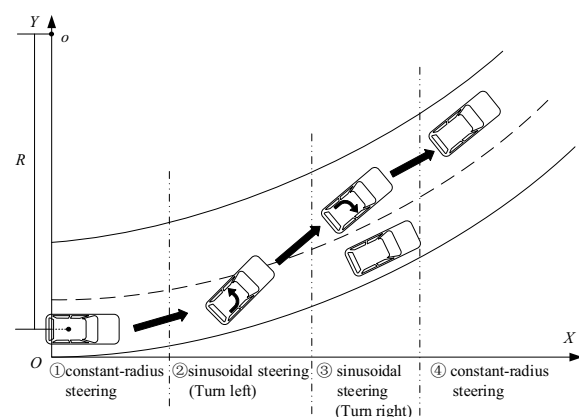


Figure 2 Diagram of vehicle lane change

behavior on straight roads can be considered as part of the same on a curved road.

A normal-distribution probability function is introduced when changing lanes on straight roads. Thus, lateral velocity is as follows:

$$v_{Yc}(t) = \frac{d}{\sqrt{2\pi}\sigma_y} \exp\left(\frac{-(4 - \mu_y)^2}{2\sigma_y^2}\right), \quad (3)$$

where v_{Yc} denotes lateral velocity of the vehicle during steering in the XOY coordinate system; d , μ_y , and σ_y denote related parameters of the vehicle's lateral velocity.

Lane-change behavior on curved roads can be decomposed into the following two states: steady-state constant-radius steering on curved roads and transient lane-change behavior on a straight road. Therefore, the vehicle's lateral movement can be considered a combination of the two states above. In the XOY coordinate system, the lateral velocity [15] is expressed as follows:

$$v_Y(t) = v_{Y0}(t) + v_{Yc}(t_c), \quad (4)$$

where v_Y denotes the vehicle's lateral velocity, and v_{Y0} denotes the vehicle's lateral velocity during steady-state constant-radius steering.

Given that the yaw angle of a vehicle is relatively low when changing lanes on curved roads at high velocities, the lateral velocity under steady-state constant-radius steering is approximately as follows:

$$v_{Y0}(t) = \frac{1}{R} \left(a_x^2 t^3 + 2a_x v_{x0} t^2 + v_{x0} \right), \quad (5)$$

where R_0 denotes the vehicle's steering radius; v_{x0} and a_x denote the vehicle's longitudinal initial velocity and longitudinal acceleration, and t denotes driving time.

In emergency lane-changing scenarios, it is difficult to ensure safety from collisions only by braking when a stationary or low-velocity vehicle appears in front. A control parameter response delay and execution error exist based on the driver response time and braking hysteresis. Therefore, a strategy combining braking and steering is adopted to avoid collisions with the vehicle in front. The vehicle longitudinal velocity v_x and longitudinal displacement x_e can be approximated as follows:

$$\begin{cases} v_x = v_{x0} + a_b(t - t_0 - t_b), \\ x_e = v_{x0}(t_0 + t_b) + \frac{1}{2}a_b(t - t_0 - t_b)^2, \end{cases} \quad (6)$$

where t_0 denotes driver response time, t_b denotes time required to step on the brake pedal and overcome the brake clearance, and a_b denotes the vehicle braking deceleration.

The critical location relation for vehicle collision avoidance can be divided into straight- and curved-section

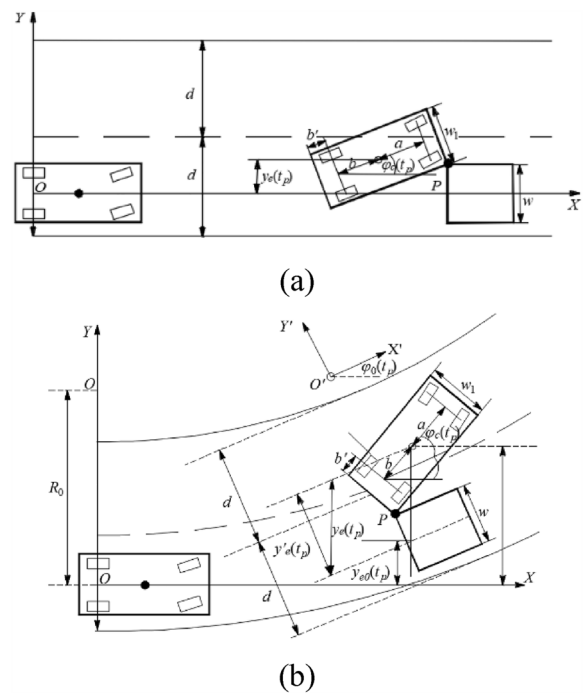


Figure 3 Critical location relation of vehicle collision avoidance: (a) Straight road condition, (b) Curved road condition

conditions. Figure 3 shows the critical location relationship for vehicle collision avoidance on straight and curved roads. In Figure 3(a), the requirement for a vehicle to avoid a collision on a straight line is that when the vehicle drives to time t_p , point P at the right front does not contact the left rear of the front vehicle. In Figure 3(b), the constant-radius steering yaw angle of the vehicle at t_p time on curved roads is $\varphi_0(t_p)$. To analyze changes in the vehicle's lateral position during lane, the $O'X'Y'$ coordinate system is introduced by rotating the OXY coordinate system $\varphi_0(t_p)$ counterclockwise at the t_p time. At this point, the angle between the longitudinal axis of the lane-change vehicle and the $O'X'$ axis is defined as the lane-change yaw angle $\varphi_c(t_p)$. The requirement for a vehicle to avoid a collision corresponds to that when the vehicle drives to time t_p , point P at the right rear does not contact the left rear of the front vehicle. Based on the position, geometry, and motion of the vehicle, the above conditions for straight and curved roads are expressed as Eqs. (7) and (8), respectively:

$$y_e(t_p) \geq \frac{w}{2} + \frac{w_1}{2} \cos(\varphi_c(t_p)) - (L - bb') \sin(\varphi_c(t_p)), \quad (7)$$

$$\begin{cases} y'_e(t_p) \geq \frac{w}{2} + [(b + b') \sin(\varphi_c(t_p)) + \frac{w'}{2} \cos(\varphi_c(t_p))], \\ y'_e(t_p) = \frac{y'_e(t_p)}{\cos(\varphi_c(t_p))} \geq \frac{w}{2 \cos(\varphi_c(t_p))} + \\ [(b + b') \tan \varphi_c(t_p) + \frac{w_1}{2}], \end{cases} \quad (8)$$

where $y_e(t_p)$ and $y'_e(t_p)$ denote the vehicle's lane-change lateral displacement at time t_p in the OXY and $O'X'Y'$ coordinate system, respectively; w denotes the front vehicle width, and w_1 denotes width of the host vehicle. In addition, L denotes length of the host vehicle. b denotes longitudinal displacement from the host vehicle mass center to the rear axle, and b' denotes the rear overhang length.

The probability that the vehicle completes the entire lane-change process in the period of sinusoidal steering and motion delay is set as p . The driving-safety control objectives are expressed as follows:

- 1) The vehicle can avoid the front vehicle to prevent collision.
- 2) Vehicle parameters can be corrected in time and lateral displacement meets adjacent lanes.
- 3) The vehicle can satisfy driving stability and its lateral acceleration should be less than the limit value to avoid sideslip or rollover.

By combining the driver's response time and the vehicle's motion response delay time, the related parameters in Eq. (3) are as follows:

$$\begin{cases} d = 3.75, \\ \mu_y = t_0 + t_b + 1/2f + t_d, \\ p = p\{\mu_y - \lambda\sigma_y < t < \mu_y + \lambda\delta_y\} = \Phi(\lambda), \\ \sigma_y = (1/f + 2t_d)/\lambda, \end{cases} \quad (9)$$

where f denotes the driver's sinusoidal steering frequency, which is generally 0.3–0.5 Hz in case of emergency steering. t_d denotes delay time of the vehicle's lateral velocity, which is related to vehicle dynamics. $\lambda \in [5, 6]$ denotes the probability coefficient, subject to $98.56\% \leq p \leq 99.84\%$.

At $t = \mu_y$, which corresponds to the pre-collision time, the lateral velocity reaches its maximum value. The lateral and longitudinal displacements of the host vehicle should be minimized to the maximum possible extent to satisfy the requirements of the critical position for collision avoidance. The critical conditions for emergency collision avoidance on straight and curved roads are expressed in Eqs. (10) and (11), respectively:

$$\begin{cases} y_e(t_p) = 3.75, \\ y_e(t_p) = \frac{w}{2} + \frac{w_1}{2} \cos(\varphi_c(t_p)_{\max}) - (L - b - b') \sin(\varphi_c(t_p)_{\max}), \\ a_Y(t)_{\max} = \frac{3.75\lambda^2}{\sqrt{2}(1/f + 2t_d)} \exp\left(-\frac{1}{2}\right) \leq a_{Y \max}, \\ \varphi_c(t_p)_{\max} = \frac{3.75\lambda^2}{\sqrt{2}(1/f + 2t_d)v_{xc}(t)|_{t=\mu_y}}, \end{cases} \quad (10)$$

$$\begin{cases} y'_e(t_p) = 3.75, \\ y_e(t_p) = \frac{w}{2} + \frac{w_1}{2} \cos(\varphi_c(t_p)_{\max}) - (L - b - b') \sin(\varphi_c(t_p)_{\max}), \\ a_Y(t)_{\max} = \frac{3.75\lambda^2}{\sqrt{2}(1/f + 2t_d)} \exp\left(-\frac{1}{2}\right) \leq a_{Y \max}, \\ \varphi_c(t_p)_{\max} = \frac{3.75\lambda^2}{\sqrt{2}(1/f + 2t_d)v_{xc}(t)|_{t=\mu_y}}. \end{cases} \quad (11)$$

As shown in Eq. (10), the maximum value of the lane-change lateral acceleration on straight roads is subject to the vehicle's initial longitudinal velocity v_{x0} , delay time of the vehicle's lateral velocity t_d , driver's steering frequency f , and probability coefficient λ . However, the maximum value of the lane-change lateral acceleration on curved roads is based on the above parameters and also to the curvature of the road R_0 . The maximum value of the lane-change yaw angle $\varphi_c(t_p)_{\max}$ is also based on the vehicle's longitudinal velocity, which determines the minimum lateral displacement $y_e(t_p)_{\min}$, point-in-time t_p , and minimum safe distance [3] of the lane-change vehicle.

Based on the minimum safe distance, the minimum safe distance for lane changing under braking conditions between the host vehicle and the front vehicle are as follows:

$$\begin{aligned} S_m &= \max \{S_b + S_c\} \\ &= \max \left\{ \int_0^t \int_0^\tau (a_b - a_0) d\tau dt + (v_{x0} - v'_{x0})\mu_y \right\}, \end{aligned} \quad (12)$$

where $S_b = \int_0^t \int_0^\tau (a_b - a_0) d\tau dt$ denotes braking distance, $S_c = (v_{x0} - v'_{x0})\mu_y$ denotes pre-collision distance, v'_{x0} denotes the front vehicle's initial longitudinal velocity; and a_0 denotes the front vehicle's initial longitudinal deceleration.

3 Three-Dimension Constraint Based Fifth-Order Polynomial Equation Lane-Change Path

In this section, a fifth-order polynomial equation lane-change path model is expressed as follows:

$$y(x) = A^T X, \tag{13}$$

with

$$\begin{cases} A = [a_0 \ a_1 \ a_3 \ a_4 \ a_5]^T, \\ X = [1 \ x \ x^2 \ x^3 \ x^4 \ x^5]^T, \end{cases} \tag{14}$$

where x , and y denote longitudinal and lateral coordinates, respectively, of the host vehicle for the collision-free path, and $a_n (n = 1, 2, \dots, 5)$ denotes the polynomial coefficient.

To ensure lane-change accuracy, the boundary constraints of the fifth-order polynomial are defined as follows:

$$\begin{cases} y(0) = 0, y(x_c) = y_c, \\ \dot{y}(0) = \dot{y}(x_c) = v_Y, \\ K(0) = K(x_c) = \rho_0, \end{cases} \tag{15}$$

where x_c and y_c denote the longitudinal and lateral coordinates of the host vehicle at the pre-collision time, respectively, and K denotes the path curvature. The values of y_c , v_Y , and ρ_0 for straight and curved roads are expressed in Eqs. (16) and (17), as follows:

$$\begin{cases} y_c = 3.75, \\ v_Y = 0, \\ \rho_0 = 0, \end{cases} \tag{16}$$

$$\begin{cases} y_c = R - [R - y'_e(t_c)] \cos(\varphi_0(t_c)), \\ v_Y = v_{Y0}, \\ \rho_0 = 1/R, \end{cases} \tag{17}$$

where $\varphi_0(t_c)$ denotes the host vehicle's constant-radius steering yaw angle on a curved road at the pre-collision time.

We substitute Eq. (13) into the constraints in Eq. (15), and Eq. (18) is obtained as follows:

$$BA = [0 \ y_c \ 0 \ 0 \ 0 \ 0]^T, \tag{18}$$

where

$$B = \begin{bmatrix} 1 & x_0 & x_0^2 & x_0^3 & x_0^4 & x_0^5 \\ 1 & x_c & x_c^2 & x_c^3 & x_c^4 & x_c^5 \\ 0 & 1 & 2x_0 & 3x_0^2 & 4x_0^3 & 5x_0^4 \\ 0 & 1 & 2x_c & 3x_c^2 & 4x_c^3 & 5x_c^4 \\ 0 & 0 & 2 & 6x_0 & 12x_0^2 & 20x_0^3 \\ 0 & 0 & 2 & 6x_c & 12x_c^2 & 20x_c^3 \end{bmatrix}.$$

Coefficient A is obtained as follows:

$$BA = [0 \ y_c \ 0 \ 0 \ 0 \ 0]^T. \tag{19}$$

Based on Eqs. (13) and (19), an equation for the desired lateral position of the vehicle track that satisfies the lane-change conditions and boundary constraints is derived as follows:

$$y(x) = 10y_c \left(\frac{x}{x_c}\right)^3 - 15y_c \left(\frac{x}{x_c}\right)^3 + 6y_c \left(\frac{x}{x_c}\right)^5. \tag{20}$$

Remark 1: The traditional steering control model [19, 22] considers only kinematic constraints. However, when emergency lane changing occurs [29], the system will be supersaturated and side-slipped, thereby leading to vehicle instability. Generally, a vehicle is in lateral stability when the actual sideslip angle tracks the desired sideslip angle. Therefore, with the exception of the kinematic constraint which is considered in the active steering control model, the yaw and lateral motions are considered in the fifth-order polynomial equation lane-changing model, that is, the three-dimensional constraint-based fifth-order polynomial equation lane-change path model, to maintain vehicle stability.

Yaw and lateral motions are developed to supplement the kinematic constraints as follows:

$$m a_Y = -2C_f(\beta + a\gamma/V - \delta) - 2C_r(\beta - b\gamma/V), \tag{21}$$

$$I_Z \dot{\gamma} = -2aC_f(\beta + a\gamma/V - \delta) - 2bC_r(\beta - b\gamma/V), \tag{22}$$

where $a\gamma = v_X\gamma + \dot{y}_Y$, β denotes the sideslip angle of the host vehicle; γ denotes the yaw rate of the host vehicle, and V denotes the velocity of the host vehicle.

The yaw rate and sideslip angle of the host vehicle are constant when the vehicle is in a stable state. Then, the desired yaw rate γ_d and sideslip angle β_d are expressed as follows:

$$\gamma_d = \frac{v_x/L}{1 + Sv_x^2} \delta, \tag{23}$$

$$\beta_d = \frac{b/L + mav_x^2/(L^2C_r)}{1 + Sv_x^2} \delta, \tag{24}$$

where L denotes the vehicle's wheelbase, and S denotes the stability factor. Generally, the lateral acceleration of a vehicle is constrained by the road adhesion coefficient, and the following relation is obtained:

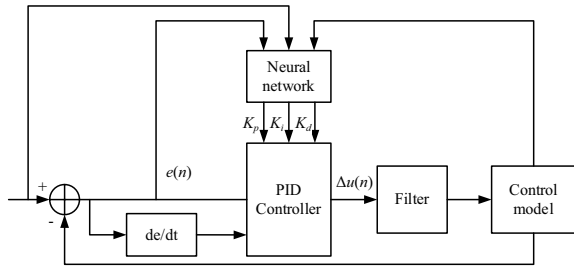


Figure 4 Constructure of the CNN controller

$$\gamma_d \leq |\gamma_{\max}| = \frac{\mu g}{v_x}, \tag{25}$$

where μ denotes the road adhesion coefficient, and γ_{\max} denotes the maximum yaw rate. Combining Eqs. (23) and (25), the correction formula of γ_d is obtained as follows:

$$\gamma_d = \min \left\{ \left| \frac{v_x/L}{1 + Sv_x^2} \delta \right|, |\gamma_{\max}| \right\} \cdot \text{sgn}(\delta), \tag{26}$$

where $\text{sgn}(\delta)$ denotes the sign function. Based on Eqs. (23), (24) and (8), the maximum value of β_d is calculated as follows:

$$|\beta_{\max}| = \mu g \left(\frac{b}{v_x^2} + \frac{ma}{C_r L} \right). \tag{27}$$

Then, β_d in Eq. (7) is expressed as follows:

$$\beta_d = \min \left\{ \left| \frac{b/L + mav_x^2/(L^2 C_r)}{1 + Sv_x^2} \delta \right|, |\beta_{\max}| \right\} \cdot \text{sgn} \left(\frac{b/L + mav_x^2/(L^2 C_r)}{1 + Sv_x^2} \delta \right). \tag{28}$$

4 Hierarchical CNNPID Controller

In this section, a hierarchical CNNPID controller that comprises two layers to avoid collisions facing emergency lane changing is constructed as shown in Figure 4, which corresponds to the lane-change path tracking PID control layer and the CNN control performance optimization layer. The error between the setting points of the lateral motion is eliminated in the lane-change path-tracking PID control layer to accurately track the lane-changing path. In the CNN control performance optimization layer, the scaled conjugate gradient backpropagation-based forward propagation control law is designed to optimize the PID control performance based on input parameters, and elastic backpropagation-based Back Propagation is adopted for weight correction.

4.1 Lane Change Path Tracking PID Control

PID control [34] is adopted to eliminate the error between the setting points of the lateral motion. A control system includes Proportional Control (P) to increase the system response rate, Integral Control (I) to minimize or eliminate the error between the setting points of the lateral motion, and control derivative (D) to reduce the overshoot/undershoot [18]. Performance controls (P), (I), and (D) are based on the values of the constants K_p , K_i and K_d . The proportional-integral-derivative (PID) controller is developed using the following input parameters: yaw rate, path, and lateral acceleration errors. This is related to the objective of minimizing the error between the predicted and desired trajectory points.

$$u(n) = K_p e(n) + K_i \sum_0^T e(n) + K_d [e(n) - e(n - 1)], \tag{29}$$

$$\Delta u(n) = u(n) - u(n - 1), \tag{30}$$

where $e(n)$ denotes the input error. We substitute Eq. (29) into the constraints in Eq. (30), and Eq. (31) is obtained as

$$\Delta u(n) = K_p [e(n) - e(n - 1)] + K_i e(n) + K_d [e(n) - 2e(n - 1) + e(n - 2)]. \tag{31}$$

Hence, Eq. (31) is simplified as follows:

$$\Delta u(n) = Ae(n) + Be(n - 1) + Ce(n - 2), \tag{32}$$

with

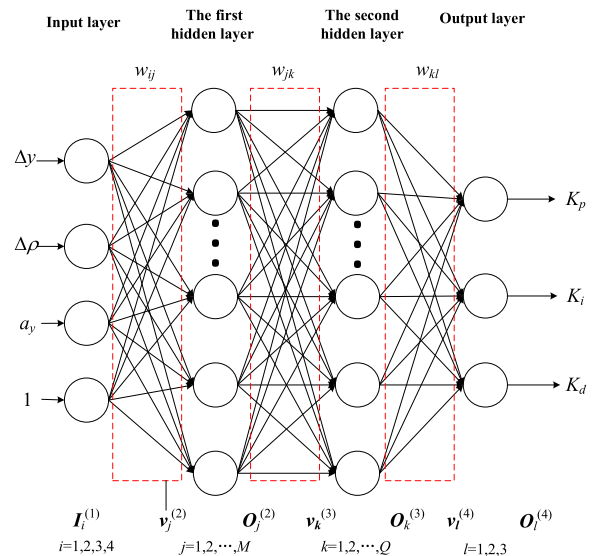


Figure 5 Neural Network architecture

$$\begin{cases} A = K_p \left(1 + \frac{T_G}{K_i} + \frac{K_i}{T_G} \right), \\ B = -K_p \left(1 + 2 \frac{K_d}{T_G} \right), \\ C = K_p \frac{K_d}{T_G}, \\ u(n) = \Delta u(n) + u(n-1). \end{cases} \quad (33)$$

4.2 CNN Control Performance Optimization

Through the calculation of the hidden layer, the three outputs correspond to the three parameters, K_p , K_i , and K_d , of the PID controller. Given that the three parameters cannot be negative, the transform function of the Neural Network in the output layer is assumed to be a nonnegative sigmoid function. The architecture of the double-hidden-layer Neural Network is shown in Figure 5. Neural nodes in the input, first hidden, second hidden, and output layers are represented by i, j, k, l , respectively. Superscripts (1), (2), (3) and (4) denote the input, first hidden, second hidden, and output layers, respectively. We assume that $Y_r[y_{rk}]$ corresponds to the actual output through forward propagation and $D_r[d_{rk}]$ corresponds to the desired output.

4.2.1 Scaled Conjugate Gradient Back-Propagation Based Forward Propagation Control Law

The input vector $I_i^{(1)}(n)$ is defined as:

$$I_i^{(1)}(n) = [\beta_d(n), e_{\beta_d}(n), a_y(n), 1], \quad i = 1, 2, \dots, N, \quad (34)$$

where the bias is treated as a weight factor with a constant input of one. N denotes the number of nodes in the input layer. The output is defined as follows:

$$O_i^{(1)}(n) = I_i^{(1)}(n), \quad (35)$$

$$O_N^{(1)}(n) \equiv 1. \quad (36)$$

The input $v_i^{(2)}(n)$ and output $O_i^{(2)}(n)$ of the first hidden layer is calculated based on the following equation:

$$v_j^{(2)}(n) = \sum_{i=0}^N w_{ij}^{(2)} O_i^{(1)}, \quad (37)$$

$$O_j^{(2)}(n) = f[v_j^{(2)}(n)], \quad j = 1, 2, \dots, M, \quad (38)$$

$$O_M^{(2)}(n) \equiv 1, \quad (39)$$

where $w_{ij}^{(2)}$ denotes the weight coefficient between the input layer and the first hidden layer, and M denotes the node number of the first hidden layer. The activation function $f(x)$ is sigmoid which is expressed as

$1/(1 - e^{-x})$. The input to the second hidden layer is denoted as follows:

$$I_j^{(1)}(n) = O_j^{(1)}(n). \quad (40)$$

The input $v_k^{(3)}(n)$ and output $O_k^{(3)}(n)$ of the second hidden layer are calculated as follows:

$$v_k^{(3)}(n) = \sum_{j=0}^M w_{jk}^{(3)} O_j^{(2)}(n), \quad (41)$$

$$O_k^{(3)}(n) = f[v_k^{(3)}(n)], \quad k = 1, 2, \dots, Q, \quad (42)$$

where $w_{jk}^{(3)}$ denotes the weight coefficient between the first and second hidden layers, and Q denotes the node number of the second hidden layer. The input of the output layer is expressed as follows:

$$I_k^{(3)}(n) = O_k^{(2)}(n), \quad (43)$$

$$O_Q^{(3)}(n) \equiv 1. \quad (44)$$

The input $v_l^{(4)}(n)$ and output $O_l^{(4)}(n)$ of the output layer are calculated as follows:

$$v_l^{(4)}(n) = \sum_{k=0}^Q w_{kl}^{(4)} O_k^{(3)}(n), \quad (45)$$

$$O_l^{(4)}(n) = g(v_l^{(4)}(n)), \quad l = 1, 2, 3. \quad (46)$$

Then

$$O_l^{(4)}(1) = K_p, O_l^{(4)}(2) = K_i, O_l^{(4)}(3) = K_d, \quad (47)$$

where $w_{kl}^{(4)}$ denotes the weight coefficient between the second hidden layer and the output layer. The activation function $g(x)$ is expressed as follows:

$$g(x) = \frac{1 + \tanh(x)}{2} = \frac{e^x}{e^x + e^{-x}}.$$

Therefore, the error signal of the k -th neuron in the output layer $e_{rk}(n)$ is as follows:

$$e_{rk}(n) = d_{rk}(n) - y_{rk}(n). \quad (48)$$

The error energy of the output neurons is defined as $e_{rk}^2(n)$. Hence, the sum of the error energies of all neurons $E(n)$ is expressed as follows:

$$E(n) = \sum_{k=1}^3 e_{rk}^2(n). \quad (49)$$

4.2.2 Elastic Back-Propagation Based Weight Correction Module

The elastic backpropagation algorithm calculates the weight corrections $\Delta w_{kl}^{(4)}(n)$, $\Delta w_{jk}^{(3)}(n)$ and $\Delta w_{ij}^{(2)}(n)$ between the output layer and second hidden layer, second hidden layer and first layer, first hidden layer, and input layer in the proper order. In the BP algorithm, weight correction is proportional to the partial differential of the energy error with respect to the weight [37]. The weight corrections $\Delta w_{kl}^{(4)}(n)$, $\Delta w_{jk}^{(3)}(n)$ and $\Delta w_{ij}^{(2)}(n)$ are expressed as follows:

$$\Delta w_{kl}^{(4)}(n) = -\eta \frac{\partial E(n)}{\partial w_{kl}^{(4)}(n)}, \quad (50)$$

$$\Delta w_{jk}^{(3)}(n) = -\eta \frac{\partial E(n)}{\partial w_{jk}^{(3)}(n)}, \quad (51)$$

$$\Delta w_{ij}^{(2)}(n) = -\eta \frac{\partial E(n)}{\partial w_{ij}^{(2)}(n)}, \quad (52)$$

$$\frac{\partial E(n)}{\partial w_{kl}^{(4)}(n)} = \frac{\partial E(n)}{\partial e_{rk}(n)} \cdot \frac{\partial e_{rk}(n)}{\partial y_{rk}(n)} \cdot \frac{\partial y_{rk}(n)}{\partial v_l^{(4)}(n)} \cdot \frac{\partial v_l^{(4)}(n)}{\partial w_{kl}^{(4)}(n)}, \quad (53)$$

$$\frac{\partial E(n)}{\partial w_{kl}^{(3)}(n)} = \frac{\partial E(n)}{\partial e_{rk}(n)} \frac{\partial e_{rk}(n)}{\partial y_{rk}(n)} \frac{\partial y_{rk}(n)}{\partial v_l^{(4)}(n)} \times \frac{\partial v_l^{(4)}(n)}{\partial v_i(n)} \frac{\partial O_k^{(3)}(n)}{\partial v_k^{(3)}(n)} \frac{\partial v_k^{(3)}(n)}{\partial w_{jk}^{(3)}(n)}, \quad (54)$$

$$\frac{\partial E(n)}{\partial w_{ij}^{(2)}(n)} = \frac{\partial E(n)}{\partial e_{rk}(n)} \frac{\partial e_{rk}(n)}{\partial y_{rk}(n)} \frac{\partial y_{rk}(n)}{\partial v_l^{(4)}(n)} \frac{\partial v_l^{(4)}(n)}{\partial O_k^{(3)}(n)} \times \frac{\partial O_k^{(3)}(n)}{\partial v_k^{(3)}(n)} \frac{\partial v_k^{(3)}(n)}{\partial O_j^{(2)}(n)} \frac{\partial O_j^{(2)}(n)}{\partial v_j^{(2)}(n)} \frac{\partial v_j^{(2)}(n)}{\partial w_{ij}^{(2)}(n)}. \quad (55)$$

The weight correction coefficient $\Delta w_{kl}^{(4)}(n)$, $\Delta w_{jk}^{(3)}(n)$ and $\Delta w_{ij}^{(2)}(n)$ are uniformly described by $R_{pq}^{(m)}(n)$. To maximize the calculation results of the last correction weight, the improved correction of correction weight is obtained by introducing the inertial coefficient α :

$$\Delta R_{pq}^{(m)}(n+1)_c = \Delta R_{pq}^{(m)}(n)_c + \alpha \Delta R_{pq}^{(m)}(n-1)_c. \quad (56)$$

Therefore, the new correction weight $R(n+1)_c$ for the next iteration is as follows:

$$R_{pq}^{(m)}(n+1)_c = \Delta R_{pq}^{(m)}(n)_c + \alpha \Delta R_{pq}^{(m)}(n)_c. \quad (57)$$

Remark 2: For traditional PID control [30, 34], if K_p is excessively high, it causes an instability overshoot and even instability in the system. Conversely, it reduces the precision adjustment and places the system in a static state so that the dynamic characteristics are lost. At a constant value of K_i , if K_i is excessively high, it will cause an overshoot of the response. In contrast, it is difficult to eliminate the steady-state error and affect the accuracy of the system. If K_d is too high, it will slow down the response, and the ability of the system will decrease.

To eliminate the effect of parameter variation on the PID control performance, a four-layer CNN architecture consisting of an input layer, two hidden layers, and an output layer is developed to optimize the PID performance according to the input data. The scaled conjugate gradient backpropagation-based forward propagation control law is designed to represent a nonlinear function and optimize the performance according to the input parameters. And elastic backpropagation-based backpropagation is adopted for weight correction.

4.3 Model Training and Testing

The design of the Neural Network is completed, and this is followed by training and testing. To ensure the superiority and reliability of the Neural Network, it is necessary to collect large quantities of rear-end driving experience data. Given that it is difficult to collect a high amount of rear-end collision avoidance data, we chose data summarized from real driving collected by the Virginia Tech Transportation Institute (VTTI) based on test security on a real road and then simulated rear-end collision avoidance [33]. Through data screening, 4000 groups of vehicle driving data that successfully completed collision avoidance are selected as the sample data. In addition, 300 groups are used for offline training and testing (3:1). After approximately 150000 steps, the training results satisfied expectations. The output error of the neural network is approximately 4.98%, which is less than the target error of 5% and meets the application requirements.

Table 1 Neural Network training parameters

System structure	Input	Hidden	Output
Number of neurons	3	30, 30	1
Transfer function	Tansg	Tansig	Purelin
Training algorithm		Trainlm	
Maximum cycle time		2000	
Learning rate		0.01	
Target error		0.1	
Maximum gradient		$1e^{-8}$	



Figure 6 Hardware-in-the-loop simulation platform



Figure 7 The appearance, interior layout of the intelligent vehicle

A schematic of the Neural Network is shown in Figure 5, and training parameters are given in Table 1.

5 Experimental Verification and Analysis

5.1 Model Training and Testing

In this section, simulation experiments and actual vehicle tests are presented to verify the effectiveness of the proposed control method for intelligent vehicles. Simulation experiments based on a hardware-in-the-loop (HIL) simulation platform with a high-fidelity full-vehicle model can verify the reliability of steering and collision avoidance in high-velocity scenarios. A real vehicle test can prove the accuracy and practicality of the tracking method under real conditions.

Figure 6 shows the HIL simulation platform which is a 6 DOF QJ-4B dynamic test platform that includes an interactive visual system, cockpit, and visual software. It can achieve a pixel view of up to 3072×168 pixels and a visual display rate of more than 24 fps. The response times of the machine operation and the visual display are less than 30 ms.

The critical experimental conditions are set on the platform. By setting up the scene, a simulator can be used to analyze the effectiveness of the vehicle control system. To ensure the safety of the test, the following methods are adopted. First, we designed a rear-end transient scene and obtained the optimal lane-changing path based on training samples. Second, a driver with more than 10 years of driving experience is selected to drive the HIL simulation platform to collect vehicle path data under the same conditions. Finally, a real vehicle reproduced the experimental scene to verify the following effect on the expected path: The intelligent vehicle model is shown in Figure 7.

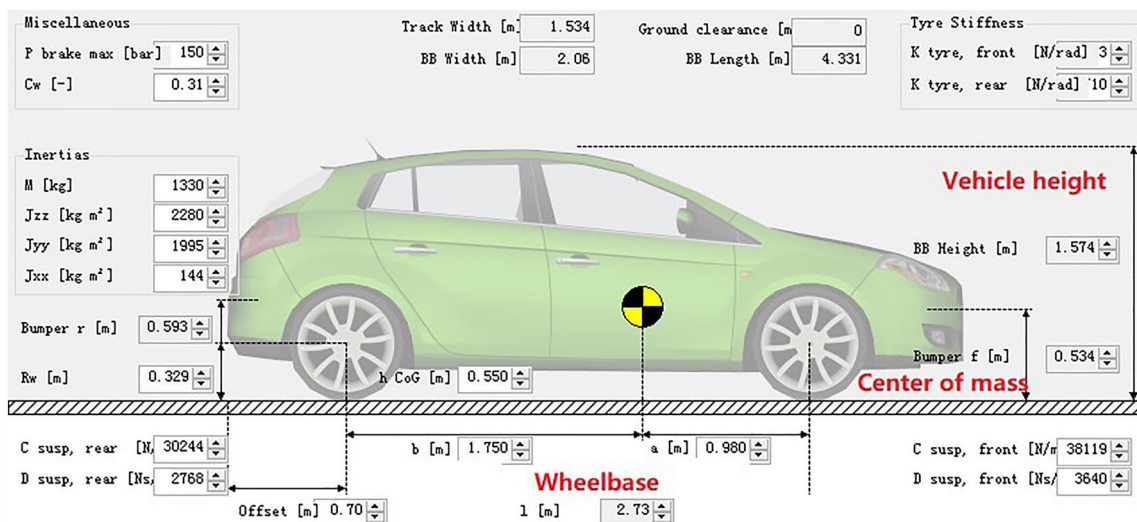


Figure 8 The static parameter setting of the vehicle

Table 2 The vehicle parameters

Parameters	Value
Vehicle preparation quality (kg)	1330
Body size (m)	BB Width=2.060 BB Length=4.331 BB Height=1.574
Wheelbase (m)	2.730
Tire stiffness (N/rad)	$C_{cr} = 92710$ $C_{cf} = 55273$
Rotational inertia around Z axis (kg·m ²)	2280

The Intelligent vehicle platform, which is converted from a Harvard off-road vehicle, is equipped with sensors, including laser radar, millimeter-wave radar, camera, and a GPS/INS integrated navigation system. The entire control system consists of a decision-making unit and a control unit. With the perception component, the functions of vehicle, lane, and obstacle identification are realized. An RT2000 GPS/INS integrated navigation system is used to measure the movement of the vehicles.

The static parameter settings of the vehicle used in the simulation experiments are shown in Figure 8. Some of the key parameters are listed in Table 2. The vehicle velocity is set to 90 km/h. To verify the effectiveness of the control method, we simulated a sudden traffic accident on a certain road section based on the HIL simulation platform. The accident occurred on a road where a vehicle passed, and we tested whether the system is able to respond to the rear-end collision transient in a timely and accurate manner. The system response acceleration, feedback response error, and other parameters are collected and compared with the results of the traditional control method.

5.2 Simulation Results and Analysis

Figure 9(a) shows the constant-radius steering response error of lateral acceleration results under the control of the PID and CNNPID controllers. For the control performance, the control errors of both methods can converge. The error control curve of PID surges from 0.1 to -0.6 m/s², and there exist two peaks based on sharp changes such as these. In addition, the error ranges from -0.6 to 0.3 m/s². In contrast, the error control curve of CNNPID is stable, with a fluctuation range of -0.2 to 0.2 m/s². In most cases, steady-state errors which are less than 0.05 m/s² satisfy the requirements of quick collision avoidance by active steering. This is due to the CNN control performance optimization layer, which eliminates the effect of parameter variation on the PID control performance.

The control error of the lateral acceleration is shown in Figure 9(b) and indicates that the linearity of the lateral acceleration under the control of the CNNPID is higher. Except the absolute overshoot at the beginning is less than 0.5 m/s², the steady-state error in the rest of the time is limited within (-0.5~0.1) m/s². Figure 9(c) shows that the CNNPID controller exhibits an excellent ability to deal with the uncertainty of acceleration changes. When compared to the PID controller, the control effect of the CNNPID controller is more stable, the steering is more accurate, and it does not require a complex algorithm or long-term training of the Neural Network.

Figure 9(d) shows the comparison of the lane-change path of the vehicle under the control of two controllers. As shown in the figure, the vehicle path controlled by CNNPID is smooth, and the overall slope changes smoothly. The vehicle's path controlled by the PID exhibits a high slope at the beginning of steering and

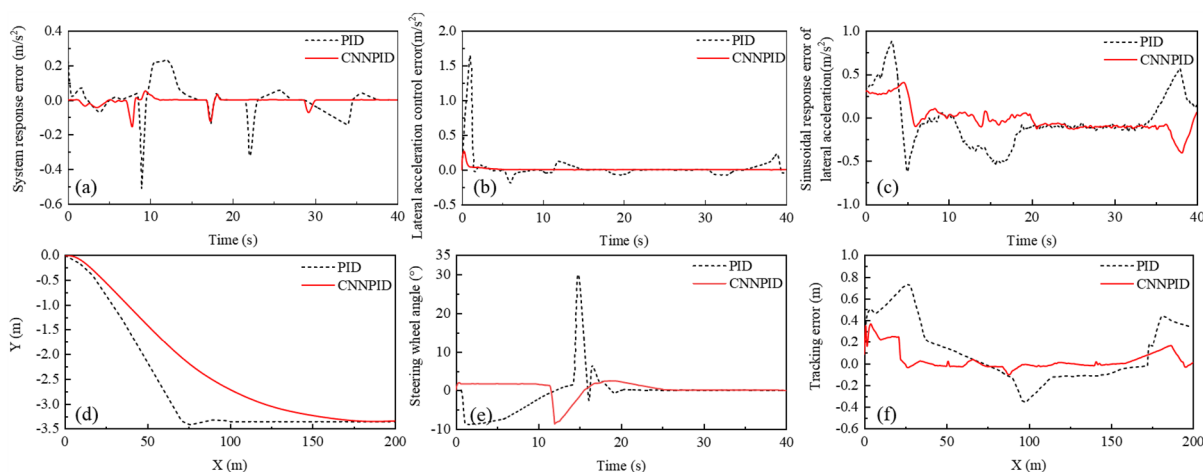


Figure 9 Results of the simulation experiments: (a)Constant-radius steering response error of the lateral acceleration, (b) Control error of the lateral acceleration, (c) Sinusoidal response error of the lateral acceleration, (d) Path of active steering, (e) Steering angle, (f) Tracking error

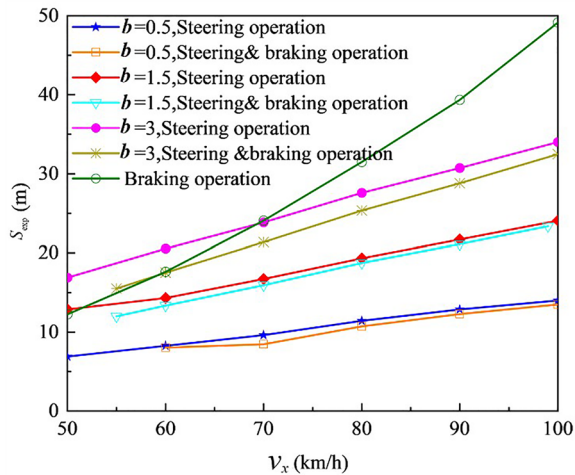


Figure 10 Minimum safe distance in different control strategy

then gradually becomes smooth. The proposed control method increases system stability.

As shown in Figure 9(e), the steering angle based on the minimum safe distance presents a stable curve. Although the system response performance decreases, some response characteristics are lost to ensure steering safety during the rear-end collision transient. The results indicate that the CNNPID control method increases the stability of the system.

Figure 9(f) demonstrates that the control system exhibits a low overshoot although the overall control results for the path are satisfactory.

The curves in Figure 10 show a comparison of the minimum safe distance of the vehicle in the rear-end collision transient where b denotes the required lateral distance. An analysis of these curves indicates that for the same lateral distance, the minimum safe distance required for the steering and braking operations exceeds that required for the steering and braking operations.

Table 3 presents a performance comparison between the PID and CNNPID control methods. As shown in the table, the error of the improved control method significantly decreases, and the control accuracy

significantly improves. This indicates that the improved control method is superior to the PID control method.

In summary, the response delay and overshoot problems of intelligent vehicles facing emergency lane changing due to variations in PID parameters are addressed. Finally, we process and analyze data obtained from 30 sets of experiments. The vehicle’s lateral performance is summarized in Table 3.

5.3 Real Vehicle Test and Analysis

Given the complexity of a real driving environment, a real vehicle test must be conducted to further verify the effectiveness and reliability of the control method. Considering the danger of transient conditions, we chose a one-way road with a relatively small traffic volume and a velocity limit of 100 km/h.

Two test conditions (a straight road scenario and a curved road scenario) are designed to verify the validity of the CNNPID controller. Seven drivers of different ages are selected to participate in the tests under each condition. Subjects 1–3 possessed 1–3 years of driving experience; subjects 4–6 possessed 3–5 years of driving experience; subject 7 possessed > 5 years of driving experience. Participants 1 and 4 are female, whereas the others are male. Road information, vehicle path, and other parameters are collected with an integrated system of inertial navigation/GPS by performing every condition several times.

Scenario on straight roads: First, we designed an active steering system for a straight road. The host vehicle is driven at a velocity of 120 km/h along the road, and the obstacle vehicle travelled in the same lane at a velocity of 72 km/h in front of the host vehicle located 50 m away.

Figure 11(a) shows the results of active steering. The target, ideal, and actual paths are shown in Figure 11(b). When combined with a detailed view of the parts marked by the red rectangle, it is observed that the consistency of each driver is high. The errors between the actual and target paths of each driver are shown in Figure 11(c). The maximum error is approximately 0.23 m. As shown in Figure 11(e) and (f), the maximum steering wheel angle and maximum lateral acceleration are approximately

Table 3 Comparison of vehicle lateral performance

Parameters	PID		CNNPID	
	Mean deviation	Standard deviation	Mean deviation	Standard deviation
The system’s response error (m/s ²)	0.1857	0.2689	0.0834	0.1365
The lateral acceleration control error (m/s ²)	0.3968	0.4536	0.0026	0.0835
The tracking error (m)	0.3694	0.7589	0.13	0.65

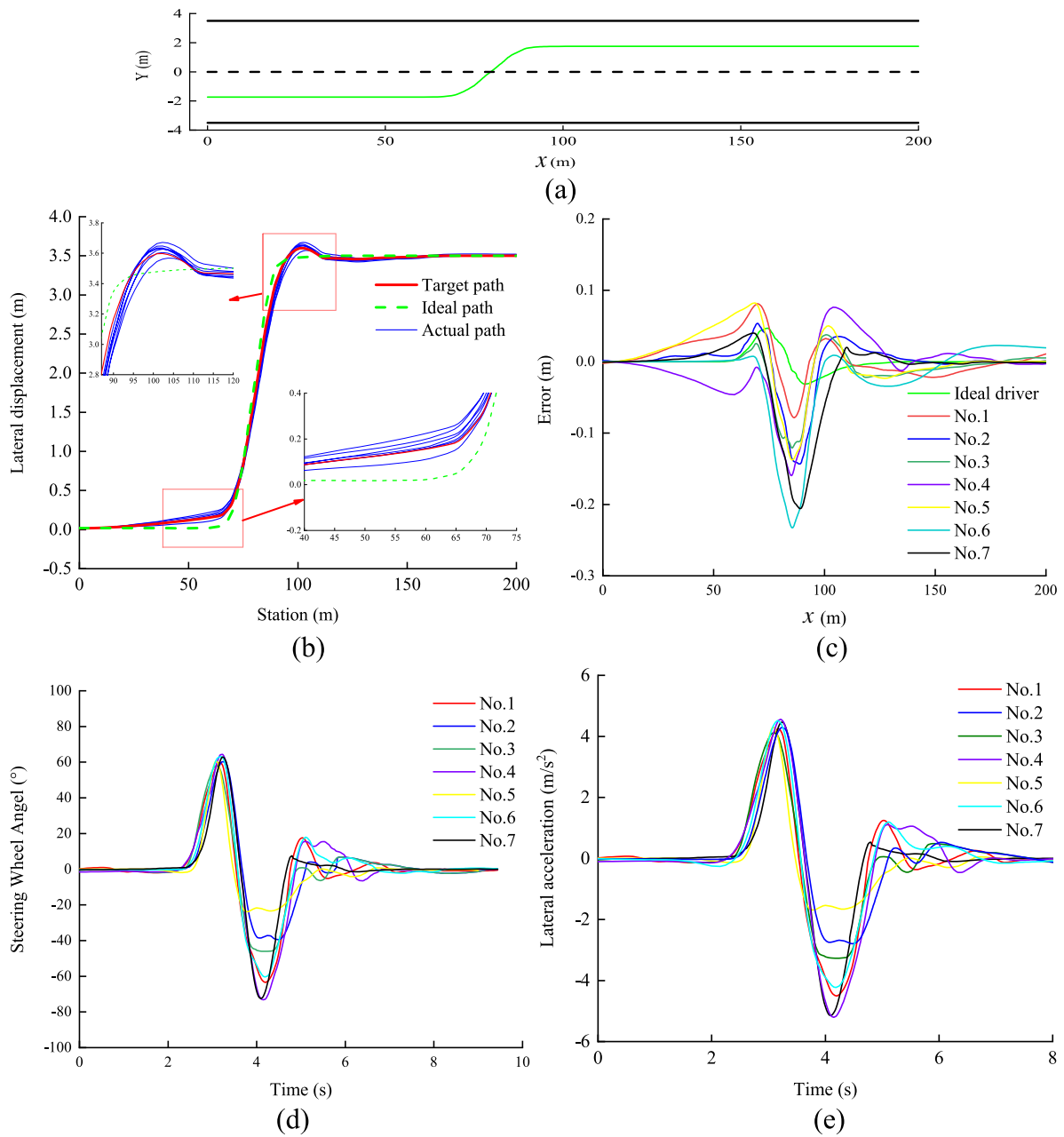


Figure 11 Results of emergency steering in a straight road: (a) Diagram of collision avoidance, (b) Vehicle's path, (c) Lateral distance error, (d) Steering wheel angle, (e) Lateral acceleration

72.99 ° and 5.19 m/s respectively. Therefore, each driver can efficiently avoid rear-end collisions.

Scenario on curved roads: We considered another active steering action on a curved road. The host vehicle is driven at a velocity of 120 km/h along the road, and the obstacle vehicle travelled in the same lane at a velocity of 72 km/h in front of the host vehicle 40 m away. The initial curvature of the road is zero and the final curvature is 0.002.

The results of the steering avoidance which indicate that the host vehicle can successfully avoid a collision are shown in Figure 12(a). The target, ideal, and actual paths are shown in Figure 12(b), and a detailed view of the parts marked with a red rectangle is shown to better demonstrate the differences between drivers during steering. The errors between the actual and target paths of each driver are shown in Figure 12(c); the maximum error is approximately 0.24 m. The maximum steering wheel

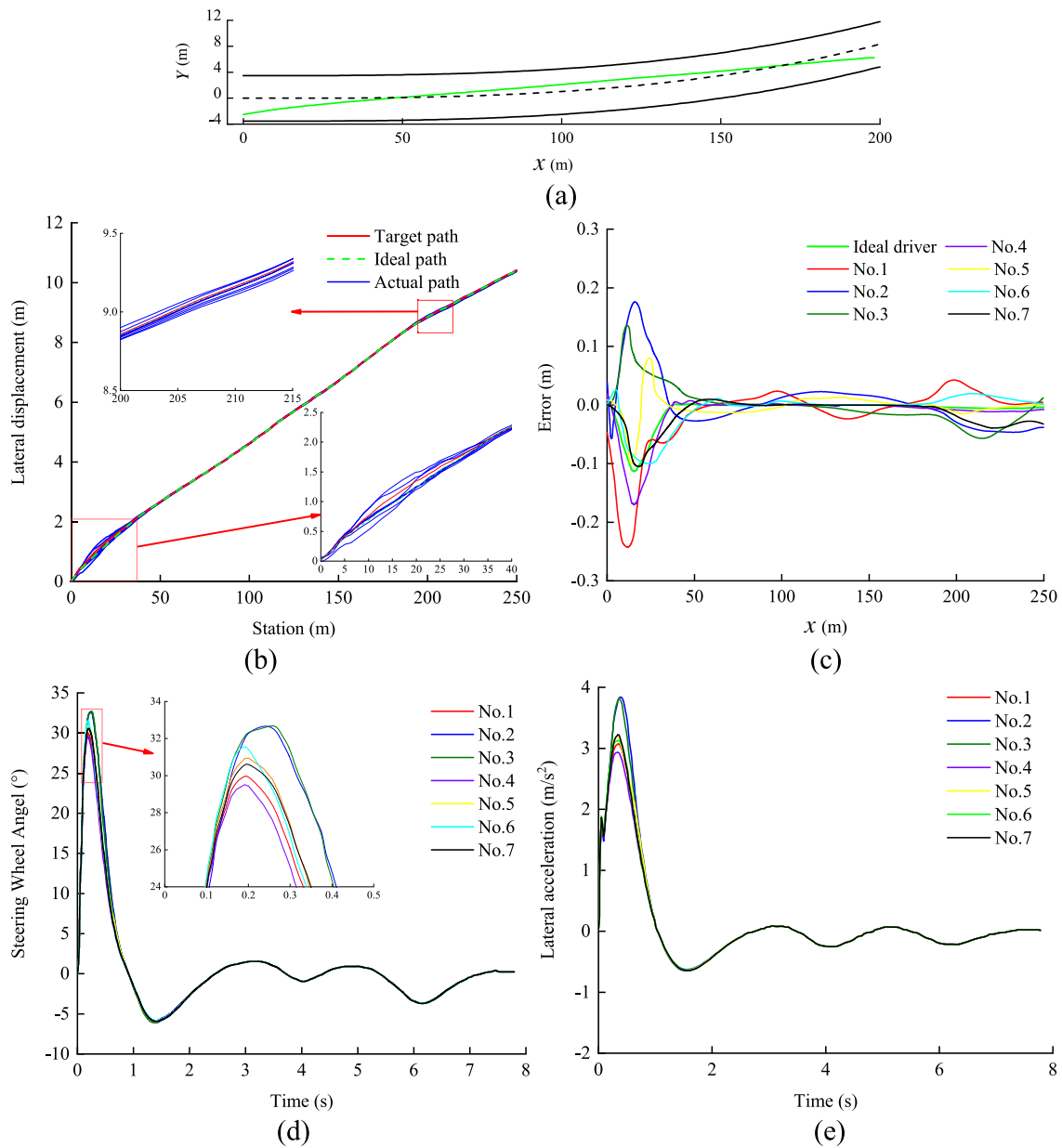


Figure 12 Results of emergency steering on a curved road: (a) Diagram of collision avoidance, (b) Vehicle's path, (c) Lateral distance error, (d) Steering wheel angle, (e) Lateral acceleration

angle and lateral acceleration are approximately 32.79° and 5.19 m/s^2 respectively, as shown in Figure 12(e) and (f), respectively. Therefore, the consistency of the steering wheel angle and lateral acceleration among the drivers improved significantly.

Next, a vehicle driven only by the driver and controlled by a PID controller is used as a comparative experiment. We used ArcMap software for data processing to analyze

the results using the three different methods. For security purposes, the host vehicle is driven at a velocity of 72 km/h along the road, and the obstacle vehicle travelled in the same lane at a velocity of 40 km/h in front of the host

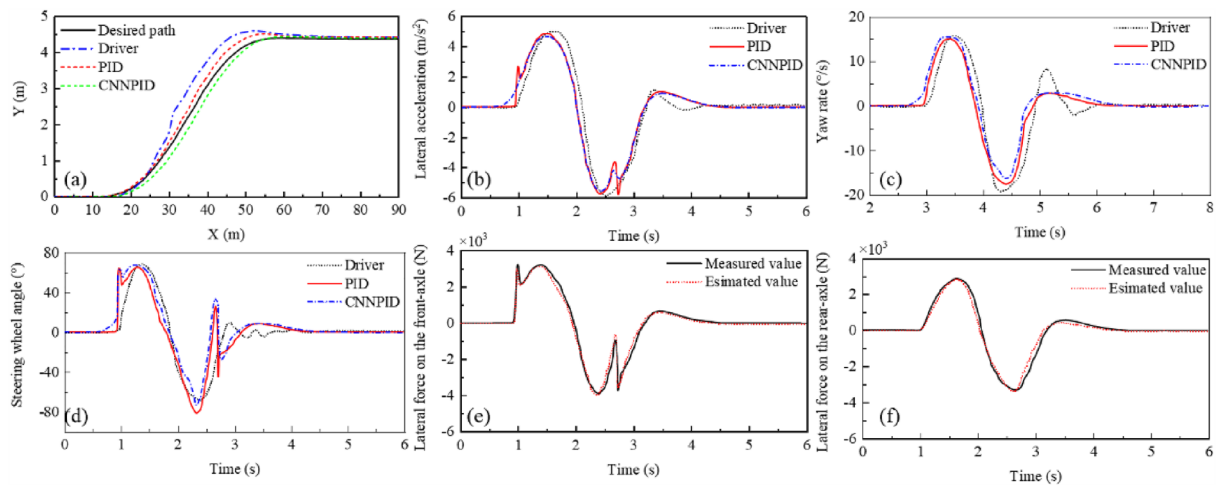


Figure 13 Results of comparative experiment: (a) Vehicle's path, (b) Lateral acceleration, (c) Yaw rate, (d) Steering wheel angle, (e) Lateral force on the front-axle of the vehicle, (f) Lateral force on the rear-axle of the vehicle

vehicle located 40 m away. The results of the comparative experiments are shown in Figure 13.

As shown in Figure 13(a), when compared with driver and PID controller, the driving path controlled by CNNPID controller is closer to the target path. The results illustrate that the proposed method can satisfy the tracking performance requirements. As shown in Figure 13(b), the peak value of lateral acceleration controlled by driver, PID controller and CNNPID controller are approximately -7.78 m/s^2 , -7.78 m/s^2 and 7.45 m/s^2 , respectively. In addition, by collating the results in Figure 13(c), it is observed that the proposed solutions exhibit superior dynamic control performance in the tracking process of the rear-end collision transient.

As shown in Figure 13(d), the steering angle controlled by the CNNPID controller exhibits fewer oscillations than those controlled by the driver and the PID controller. The peak value of the disturbance is approximately a quarter of the peak steering angle controlled by the CNNPID controller.

As shown in Figure 13(e) and (f), the estimated values of the lateral forces on the front and rear axles converge consistently to the measured value.

In summary, the proposed controller precisely follows the rear-end collision avoidance path in a real vehicle test.

6 Conclusions and discussion

The following conclusions are obtained:

- (1) An active steering control method for intelligent vehicles based on CNNPID in the rear-end collision transient under emergency lane-changing is devel-

oped to resolve response delay and overshoot problems of intelligent vehicles facing emergency lane-changing due to PID parameter variation.

- (2) We constructed a normal distribution probability function, steady constant radius steering, and instantaneous lane-change-based active steering control model for straight and curved roads. Based on this, a three-dimensional constraint-based fifth-order polynomial equation lane-change path is designed to address the stability problem with supersaturation and sideslip given emergency lane changing. Furthermore, a Hierarchical CNNPID Controller comprising two layers is constructed. The extensibility and advantages of the proposed hierarchical CNNPID control method are illustrated through comparison studies. This corresponded to a significant breakthrough in successfully addressing this challenging issue in the context of rear-end collision control.
- (3) Future research will further consider complex scenes such as the parallel operation of multiple vehicles. In addition, it is necessary to focus on the modeling of the intelligent vehicle's longitudinal velocity control, the sensitivity of different control systems to different adhesion coefficients, variable curvature path tracking, and inconsistencies in road adhesion coefficients.

Acknowledgements

The author would like to thank Yu Yang (SAIC) for providing technical support.

Author contributions

WW was in charge of the entire trial; JL wrote the manuscript; and CP and LC assisted with the sampling and laboratory analyses. All the authors have read and approved the final version of the manuscript.

Authors' Information

Wensa Wang born in 1995, is currently a Ph.D. candidate in *Transportation Engineering, Jiangsu University, China*. She received her Master's degree from *Jiangsu University* in 2020. Her research interests include intelligent vehicle controls and traffic safety.

Jun Liang born in 1976, is currently a professor and director at *Institute of Transportation Big Data and Security Control, Jiangsu University, China*. He is also a member of the Youth Expert Committee of China Intelligent Transportation Association. His research interests include intelligent transportation systems and vehicles.

Chaofeng Pan born in 1979, is currently a professor at *Jiangsu University, China*. He is one of the candidates for the selection of high-level talent from the "six Talent Peaks" in Jiangsu Province. His research interests include efficiency optimization and the energy management of electric vehicle power systems. Long Chen born in 1958, is currently a professor and PhD supervisor at *Jiangsu University, China*. He received the B.S. and PhD degrees from *Jiangsu University, China* in 1982 and 2006, respectively. His research interests include road traffic safety and management, active vehicle safety technologies, and dynamic vehicle simulations and controls. He is a recipient of the Chinese Mechanical Industry Young Scientist Award for Excellence, the Young and Middle-Aged Expert Award for Outstanding Contribution to Jiangsu Province, and the Jiangsu Provincial Science and Technology Progress Award.

Funding

Supported by National Key R&D Program of China (Grant No. 2018YFB1600500), and Jiangsu Provincial Postgraduate Research & Practice Innovation Program of (Grant No. KYCX22_3673).

Availability of data and materials

The datasets used during the current study are available from the corresponding author on reasonable request.

Declarations

Competing Interests

The authors declare that they have no competing interests.

Received: 18 October 2021 Revised: 27 July 2023 Accepted: 27 July 2023

Published online: 01 September 2023

References

- G Tiwari, D Mohan. *Transport planning and traffic safety: making cities, roads, and vehicles safer*. Boca Raton: Taylor & Francis Group: The CRC Press, 2016.
- F Wang, D F Araújo, Y F Li. Reliability assessment of autonomous vehicles based on the safety control structure. *Proceedings of the Institution of Mechanical Engineers, Part O: Journal of Risk and Reliability*, 2023, 237(2): 389-404.
- Z X Shi, J B Feng, Y X Wang. Design of vehicle steering lane change control system based on ANFIS and MPC. *Modern Manufacturing Engineering*, 2022, 2: 70-78.
- P Bansal, K M Kockelman. Forecasting Americans' long-term adoption of connected and autonomous vehicle technologies. *Transportation Research Part A: Policy and Practice*, 2017, 95: 49-63.
- P Jiang, Z Q Shen, R X Xu. Preface: Key technologies for enhancing the performance of FAST. *Research in Astronomy and Astrophysics*, 2020, 20(5): 3-4.
- E D Çetinoğlu, A G Dilektaşlı, N A Demir. The relationship between driving simulation performance and obstructive sleep apnoea risk, daytime sleepiness, obesity and road traffic accident history of commercial drivers in Turkey. *Sleep & Breathing*, 2015, 19: 865-872.
- M Guo, S Li, L Wang, et al. Research on the relationship between reaction ability and mental state for online assessment of driving fatigue. *International Journal of Environmental Research & Public Health*, 2016, 13: 11-74.
- Y Wang, K Chen, L Hu. Killer tailgating: Recommendation of traveling intervals between consecutive motor vehicles for rear-end collision avoidance. *Arabian Journal for Science & Engineering*, 2012, 37: 619-630.
- A Tawari, S Martin, M M Trivedi. Continuous head movement estimator for driver assistance: issues, algorithms, and on-road evaluations. *IEEE Transactions on Intelligent Transportation Systems*, 2014, 15(2): 818-830.
- W Zhang, C Y Zhang, W Li. Intelligent path tracking control for plant protection robot based on fuzzy PD. *International Conference on Advanced Robotics and Mechatronics IEEE*, Hefei, China, August, 2017: 27-31.
- L Song, H Guo, F Wang, et al. Model predictive control oriented shared steering control for intelligent vehicles. *29th Chinese Control and Decision Conference (CCDC)*, Chongqing, China, May 28-30, 2017: 7568-7573.
- B A Guvenc, L Guvenc, K Karaman, et al. Robust yaw stability controller design and hardware-in-the-loop testing for a road vehicle. *IEEE Transactions on Vehicular Technology*, 2014, 58(2): 555-571.
- M Yue, X Hou, M Fan, et al. Coordinated trajectory tracking control for an underactuated tractor-trailer vehicle via MPC and SMC approaches. *2nd International Conference on Advanced Robotics and Mechatronics (ICARM)*, Singapore, July 18-20, 2018: 82-87.
- M Kabiri, H Atrianfar, M B Menhaj. Trajectory tracking of a class of under-actuated thrust-propelled vehicle with uncertainties and unknown disturbances. *Nonlinear Dynamics*, 2017, 90(3): 1695-1706.
- C L Wang, C C Hwang, J Y Hung. Path tracking of an automatic ground vehicle with different payloads by hierarchical improved fuzzy dynamic sliding-mode control. *IEEE Transactions on Fuzzy Systems*, 2017, 26(2): 899-914.
- C Zhang, J Hu, J Qiu, et al. A novel fuzzy observer-based steering control approach for path tracking in autonomous vehicles. *IEEE Transactions on Fuzzy Systems*, 2018, 27(2): 278-290.
- F Tian, Z Li, F Y Wang, et al. Parallel learning-based steering control for autonomous driving. *IEEE Transactions on Intelligent Vehicles*, 2022, 8(1): 379-389.
- A D Sabiha, M A Kamel, E Said, et al. ROS-based trajectory tracking control for autonomous tracked vehicle using optimized backstepping and sliding mode control. *Robotics and Autonomous Systems*, 2022, 152: 104058.
- J Liu, P Jayakumar, J L Stein, et al. A study on model fidelity for model predictive control-based obstacle avoidance in high-velocity autonomous ground vehicles. *Vehicle System Dynamics*, 2016, 54(11): 1629-1650.
- A Tealab. Time series forecasting using artificial Neural Networks methodologies: A systematic review. *Future Computing and Informatics Journal*, 2018, 3(2): 334-340.
- C Katrakazas, M Quddus, W H Chen, et al. Real-time motion planning methods for autonomous on-road driving: State-of-the-art and future research directions. *Transportation Research Part C: Emerging Technologies*, 2015, 60: 416-442.
- E Lucet, R Lenain, C Grand. Dynamic path tracking control of a vehicle on slippery terrain. *Control Engineering Practice*, 2015, 42: 60-73.
- X Xiong, L Chen, J Liang. A new framework of vehicle collision prediction by combining SVM and HMM. *IEEE Transactions on Intelligent Transportation Systems*, 2018, 19(3): 1-12.
- F Biondi, D L Strayer, R Rossi, et al. Advanced driver assistance systems: Using multimodal redundant warnings to enhance road safety. *Applied Ergonomics*, 2017, 58: 238-244.
- W Peng. Research on optimization and implementation of BP Neural Network Algorithm. *7th International Conference on Intelligent Computation Technology and Automation*, Changsha, China, October 25-26, 2014: 104-107.
- Y Koubaa, M Boukattaya, T Dammak. Adaptive sliding-mode dynamic control for path tracking of nonholonomic wheeled mobile robot. *Journal of Automation and Systems Engineering*, 2015, 9(2): 119-131.
- Z Shuai, H Zhang, J Wang, et al. Combined AFS and DYC control of Four-wheel-independent-drive electric vehicles over CAN Network with time-varying delays. *IEEE Transactions on Vehicular Technology*, 2014, 63(2): 591-602.
- J Zhang, H Wang, J Zheng, et al. Adaptive sliding mode-based lateral stability control of steer-by-wire vehicles with experimental validation. *IEEE Transactions on Vehicular Technology*, 2020, 69(9): 9589-9600.

- [29] L Hong, Y Sun, C Cao. Motor synchronization control for multistage hot die forging press feed manipulator based on BP-PID controller. *International Journal of Computing Science and Mathematics*, 2020, 11(4): 347-356.
- [30] G Huang, X Yuan, K Shi, et al. A BP-PID controller-based multi-model control system for lateral stability of distributed drive electric vehicle. *Journal of the Franklin Institute*, 2019, 356(13): 7290-7311.
- [31] J Baek, C Kang, W Kim. Practical approach for developing lateral motion control of autonomous lane change system. *Applied Sciences*, 2020, 10(9): 1-15.
- [32] A Wasala, D Byrne, P Miesbauer, et al. Trajectory based lateral control: A Reinforcement Learning case study. *Engineering Applications of Artificial Intelligence*, 2020, 94(2): 1-13.
- [33] Y Jie, Q Wang, L Yuan. An improved second order sliding mode twisting algorithm for finite-time trajectory tracking of intelligent vehicle. *Advances in Mechanical Engineering*, 2013(4): 1-8.
- [34] S Chen, G Xiong, H Chen, et al. MPC-based path tracking with PID velocity control for high-velocity autonomous vehicles considering time-optimal travel. *Journal of Central South University*, 2020: 1-19.
- [35] Z He, L Nie, Z Yin, et al. A two-layer controller for lateral path tracking control of autonomous vehicles. *Sensors*, 2020, 20(13): 1-20.
- [36] C Hu, Z Wang, H Taghavifar, et al. MME-EKF-based path-tracking control of autonomous vehicles considering input saturation. *IEEE Transactions on Vehicular Technology*, 2019, 68(6): 5246-5259.
- [37] C Chen, X Liu, H H Chen, et al. A rear-end collision risk evaluation and control scheme using a Bayesian Network Model. *IEEE Transactions on Intelligent Transportation Systems*, 2018, 20(1): 1-21.
- [38] X Ji, X He, L Chen, et al. Adaptive-neural-network-based robust lateral motion control for autonomous vehicle at driving limits. *Control Engineering Practice*, 2018, 76: 41-53.
- [39] S Xu, H Peng. Design, analysis, and experiments of preview path tracking control for autonomous vehicles. *IEEE Transactions on Intelligent Transportation Systems*, 2020, 21(1): 48-58.
- [40] S Yang, L Xi, J Hao, et al. Aerodynamic-parameter identification and attitude control of Quad-Rotor model with CIFER and adaptive LADRC. *Chinese Journal of Mechanical Engineering*, 2021, 34(1): 1.
- [41] X Tang, Z Zhang, Y Qin. On-road object detection and tracking based on radar and vision fusion: A review. *IEEE Intelligent Transportation Systems Magazine*, 2021: 2-27.
- [42] W S Wang, J Liang, C F Pan, et al. NLS based hierarchical anti-disturbance controller for vehicle platoons with time-varying parameter uncertainties. *IEEE Transactions on Intelligent Transportation Systems*, 2022, 23(11): 21062-21073.

Submit your manuscript to a SpringerOpen[®] journal and benefit from:

- Convenient online submission
- Rigorous peer review
- Open access: articles freely available online
- High visibility within the field
- Retaining the copyright to your article

Submit your next manuscript at ► [springeropen.com](https://www.springeropen.com)
